Eur. Phys. J. D **44**, 81–91 (2007)
DOI: 10.1140/epjd/e2007-00137-2

THE EUROPEAN PHYSICAL JOURNAL D

Non-monotonic size effects on the structure and thermodynamics of Coulomb clusters in three-dimensional harmonic traps

F. Calvo[1,a] and E. Yurtsever[2]

[1] Laboratoire de Chimie et Physique Quantiques, IRSAMC, Université Paul Sabatier, 118 route de Narbonne, 31062 Toulouse Cedex, France
[2] Koç University, Rumelifeneriyolu, Sariyer, 34450 Istanbul, Turkey

Received 20 October 2006 / Received in final form 12 January 2007
Published online 28 March 2007 –

Abstract. Finite-size effects on the static and thermodynamical properties of small three-dimensional clusters of identical charged particles confined by an harmonic trap are investigated using global optimization and numerical simulations. The relative stabilities of clusters containing up to 100 particles are estimated from the second energy derivatives, as well as from the energy gap between the two lowest-energy structures at a given size. We also provide a lower bound for the number of permutationally independent minima, as a function of size, up to $n = 75$. Molecular dynamics and exchange Monte Carlo simulations are performed to get insight into the finite temperature behaviour of these clusters. By focusing on specific sizes, we illustrate the interplay between the stable structures, the possible competition between different isomers, and the melting point. In particular, we find that the orientational melting phenomenon known in two-dimensional clusters has an equivalent form in some three-dimensional clusters. The vibrational spectra, computed for all sizes up to 100, shows an increasing number of low-frequency modes, but comparing to hydrodynamical theory reveals strong correlation effects. Finally, we investigate the effects of the trap anisotropy on the general shape of Coulomb clusters, and on the melting point of a selected case.

PACS. 36.40.Mr Spectroscopy and geometrical structure of clusters – 36.40.Ei Phase transitions in clusters – 64.60.Cn Order-disorder transformations; statistical mechanics of model systems – 68.65.-k Low-dimensional, mesoscopic, and nanoscale systems: structure and nonelectronic properties

1 Introduction

Recent progresses in trap technologies have allowed clusters containing up to hundred thousands of charged particles to be studied over relatively long time scales [1–3]. In the Drewsen group, large clusters of identical ions (the so-called one-component plasma) stabilized in linear Paul traps have been shown to form Coulomb crystals with well-defined layer structures [2,4,5]. These authors have also investigated the structure in two-component crystals [6], and the structural transitions, including melting, induced by varying the trap parameters [7] or its frequency [8]. Large crystals provide a convenient reservoir for cold atomic or molecular ions [9] that could be used for other applications. Small sets of ions in well controlled structural and thermodynamical states, especially when arranged in strings, are promising in various fields, such as high resolution spectroscopy [10], frequency standards [11] or quantum information [12,13].

Historically, the magnetic Penning trap was first used to confine ions in clusters and cooling them down to stabilize them [14]. Three-dimensional crystals of charged particles can also be obtained using micrometer-sized polymer particles, that are suspended in a radio-frequency gas discharge [3,15]. Such mesoscopic particles carry a much higher charge with respect to ions or molecules, which leads to the formation of stable, crystal-like structures at room temperature, while trapped ions form ordered structures only at millikelvins, hence requiring assistance of electron or laser cooling. However, the Coulomb interaction is affected (shielded) by the presence of opposite charges in the plasma created upon electric discharge. Yet, their larger individual size allow the clusters to be directly visualized.

From a fundamental point of view, clusters of trapped ions constitute a laboratory for studying the behaviour of matter at the finite size scale. In very few cases, analytical theories have been developed [16,17]. However, and not surprisingly, computer simulations have been much more employed to assist in interpreting experiments, sometimes anticipating them. Several groups have used numerical methods to locate the most stable configurations of confined charges interacting through the bare [18–23] or shielded [24] Coulomb forces. Saddle configurations and rearrangement pathways have been studied by Wales and Lee [21]. Molecular dynamics (MD) simulations have been employed [25–28] to determine the structure as well, but

[a] e-mail: fcalvo@lasim.univ-lyon1.fr

also the thermodynamic stability usually characterized by the coupling parameter $\Gamma = Z^2e^2/4\pi\varepsilon_0 a_{\rm WS}k_{\rm B}T$ [29,30]. The Wigner-Seitz radius $a_{\rm WS}$, related to the density ρ through $4\pi a_{\rm WS}^3/3 = 1/\rho$, plays thus a role comparable to the temperature T. In the bulk one-component plasma, the crystal melts when Γ approaches the approximate value $\Gamma \simeq 170$ from above [29,31], or an equivalent melting temperature $T_{\rm melt} = 1/170$ as measured in reduced units.

Finite systems usually melt at lower temperatures than bulk systems [32], hence the critical parameter for a cluster of trapped ions is expected to be larger. In his molecular dynamics simulations of clusters containing 10^2, 10^3, and 10^4 ions, Schiffer recently estimated the melting temperature to be approximately 1/500, 1/278, and 1/209, respectively [27]. He also found that the scaling of $T_{\rm melt}$ with cluster size depends on the fraction of ions in the outer layer, such that the difference with the bulk melting temperature scales with that fraction. This is exactly expressed as a function of the number n of particles as $\Delta T_{\rm melt}(n) \approx n^{-1/3}$, which is also proportional to the inverse radius of the cluster. Such a scaling law is well-known in the physics of atomic and molecular clusters [33]. Another expected feature of small systems is the stronger and nonmonotonic size dependence of physical properties as the size further decreases below a certain threshold [34]. For example, the variations in the melting point of small sodium clusters can reach several tens of kelvin between two neighbouring sizes [35]. Because they were obtained on a very limited set of size, the results of Schiffer [27] could not provide any evidence for such nontrivial effects. In the 2D case, several numerical studies [36,37] including our previous work [38] have reported significant finite size effects in the melting of trapped ion clusters, particularly for heterogeneous systems.

As shown by Berry, Wales, and their coworkers [39,40], there is a very strong interplay between the structure of a cluster and its dynamical and thermodynamical behaviours. In fact, the equilibrium thermodynamics of a cluster is completely characterized by the topography of its potential energy surface, or energy landscape [41]. Even for simple interactions, the landscape can be quite complicated and exhibit several basins or funnels in competition with each other. This can give rise to a very rich thermodynamic phenomenology, where the transition between the single stable structure (the solid state) at zero temperature can evolve toward a fully melted state at high temperatures through several possible phases, including surface melting [42] or surface reconstruction [43], multistep melting [44] and more generally structural transitions [45]. A good illustration of these various phenomena is found in Lennard-Jones clusters [42,43,45,46].

The present paper focuses on finite size effects in the structural and thermodynamical properties of three-dimensional clusters of charged particles confined by harmonic traps. Most of this paper deals with isotropic traps. Beyond the geometries of the lowest-energy structures, we have chosen to investigate other aspects of the global minima, such as their stability as measured by the energy gap to the second minimum. The search for isomers other than the most stable allowed us to estimate a lower bound for the number of permutationally independent isomers as a function of increasing size. This number, which is thought to increase exponentially with size [41,47], is also directly affected by the interaction between particles, especially its range [41,48]. As will be shown below, the number of minima for trapped ion clusters also approximately follows an exponential law as the size increases.

The finite temperature behaviour was explored numerically using both molecular dynamics and Monte Carlo (MC) simulations, and computing the canonical heat capacities and root mean square bond length fluctuation, also known as the Lindemann index. As was observed for two-dimensional clusters [38] these two methods provide different but complementary information about melting in the clusters. The latter quantity is very sensitive to the relative motion of the particles in their shells, even though the shells remain rigid. Conversely, the heat capacity is sensitive to the presence of several isomers on the potential energy surface, and is the natural quantity to consider to probe the equilibrium thermodynamics of the phase transitions rounded by size effects. By performing systematic quenches of configurations gathered during the Monte Carlo trajectories, we also relate the features in the caloric curves to the properties of the underlying energy landscape.

Another goal of the present paper is to determine the vibrational modes of the trapped ion clusters and their size dependence. Several groups have investigated the normal modes and vibrational spectrum of two-dimensional clusters [49–53]. In particular, the Peeters group has recently shown that several modes exist with a frequency which is nearly independent on the number of particles [52]. The vibrational modes in three-dimensional clusters of charged particles have also received a significant attention in the theoretical community, especially from Dubin and Schiffer [54–56] but not only [57]. The former cited authors developed an hydrodynamic theory to account for the surface oscillations of a cluster of trapped ions, and investigated the effects of correlations between particles, that are not described in the continuous theory [54–56]. As we show below, the vibrations in small three-dimensional clusters are not well described by the hydrodynamic theory, even though some features such as the constant breathing frequency are well reproduced.

Finally, we have also investigated the effects of trap anisotropy on the shape of small clusters, in the regime where finite-size effects could be expected. As the trap anisotropy is varied from low to high values, the cluster shape changes from string-like to helicoidal, prolate ellipsoidal, spherical, oblate ellipsoidal, then disc-like. These structural transitions have been studied numerically by Schiffer [58] and analytically by Dubin [17]. Here, we also look at the more specific effects of size, and we determine the magnitude of cluster size effects at the resolution of single particles on the general shape diagram. Finally, we also illustrate on a specific case how the anisotropy of the trap can affect the melting temperature of the cluster.

The article is organized as follows. In the next section, we briefly describe the model and methods used to search for the stable structures and different isomers of a given cluster size, as well as some details about the numerical simulations. The results on structural and thermodynamical properties of clusters confined in an isotropic trap are given and discussed in Section 3, while our results on clusters in anisotropic traps are presented in Section 4. Some concluding remarks are finally given in Section 5.

2 Methods

n identical, particles with the same mass m and charge $q = Ze$ are confined into a harmonic, but possibly anisotropic trap potential with frequency ω_0, so that the resulting potential energy E of configuration $\mathbf{R}$ is written in physical units as

$$E(\mathbf{R}) = \sum_{i<j} \frac{Z^2e^2}{4\pi\varepsilon_0 r_{ij}} + \frac{1}{2}\sum_i m\omega_0^2\left(x_i^2 + y_i^2 + \rho z_i^2\right). \quad (1)$$

In this equation, x_i, y_i, z_i are the Cartesian coordinates of particle i in the centre of mass reference frame, and r_{ij} is the distance between particles i and j, and ρ is the non-dimensional anisotropy parameter. In most of this work, an isotropic trap ($\rho = 1$) is chosen, but ρ will be allowed to vary in Section 4. It is more convenient to work in reduced units, by normalizing the energy to E_0 and the distances to r_0 with

$$E_0 = \left[m\omega_0^2\left(\frac{Z^2e^2}{4\pi\varepsilon_0}\right)^2\right]^{1/3}, \quad (2)$$

and

$$r_0 = \left[\frac{1}{m\omega_0^2}\frac{Z^2e^2}{4\pi\varepsilon_0}\right]^{1/3}, \quad (3)$$

respectively. The temperature scale is then fixed by E_0/k_B or its inverse Γ known as the coupling parameter. The frequency unit is naturally given by ω_0. In the following, we use reduced units for all these quantities, energies being expressed in E_0, temperatures in $1/\Gamma = E_0/k_\mathrm{B}$, radii in r_0, etc. Using reduced units also enables comparison with previous work on infinite or finite one-component plasma systems.

The stable structures were located with the basin-hopping (or Monte Carlo+minimization) method [59], using a conjugate gradient procedure for local optimizations. For each size a basin-hopping search consisted of 10 000 quenches, with a particle step size of 1 unit of distance. Due to the long range of the Coulomb interaction, the number of permutationally independent isomers is much smaller for the present confined clusters than for, say, Lennard-Jones clusters [41]. By repeating the global optimization search a large number of times, many isomers could be gathered. All isomers were checked to be real minima, and were further sorted according to their potential energy and mean square radius.

The finite-temperature behaviour was investigated by performing classical, constant-energy molecular dynamics simulations, as well as exchange Monte Carlo (or parallel tempering) simulations in the canonical ensemble. The velocity Verlet method was used to propagate the cluster configuration and velocities, with a time step of 0.025 units. The initial conditions were chosen to reach a specific total energy, without inducing any linear or angular momentum. For each total energy, several runs of 10^6 steps were accumulated, following 10^5 steps left out for equilibration.

Exchange Monte Carlo simulations were carried out using 50 replicas, with temperatures allocated in a geometric progression. For each replica, 10^6 MC cycles were collected for the statistical averages after 10^5 equilibration cycles. Configurations of replicas were occasionally exchanged with 10% probability. The replicas exchanging their configurations were selected using the recent all-exchange strategy [60]. A set of 1000 configurations periodically saved for all replicas were quenched, in order to relate the variations in the thermal averages and heat capacity to the topography of the potential energy surface.

3 Results for isotropic traps

In this section, we give our main results for the structural and thermodynamical properties of ions confined by an isotropic harmonic trap, as inferred from our optimization and simulation methods.

3.1 Structure and stability

Three-dimensional clusters of trapped charged ions generally exhibit onion-ring structure with multiple shells [18–22], but also crystal-like (bcc) structures above 10^4 ions [23]. The shell structure is also well-known in two-dimensional Wigner clusters (see [38] and references therein), where it leads to different types of motion involving either orientational (or angular) or intershell (or radial) displacements. The orientational motion occurs in general at low energies or temperatures, which is consistent with low energy barriers [21,38]. Conversely, intershell motion is more closely related to melting, and requires a higher temperature, as also indicated by higher energy barriers for rearrangements [21,38].

We have determined the global minima of 3D ions in an isotropic harmonic trap containing up to $n = 100$ identical particles, as well as a large set of isomers for each cluster size. In the following, the energy of isomer i of a n-particle cluster is denoted as $E_i(n)$, with the global minimum standing as $i = 1$ or being simply denoted as $E(n)$. For convenience, we also describe the stable geometries as a series of integer numbers $(n_1, n_2, ...)$ characterizing the number of particles in a given shell, from the core to the outer shells.

Our results for the lowest energy structures agree with the results of Beekman and coworkers [22], and will not be detailed further. Instead we address the issue of relative

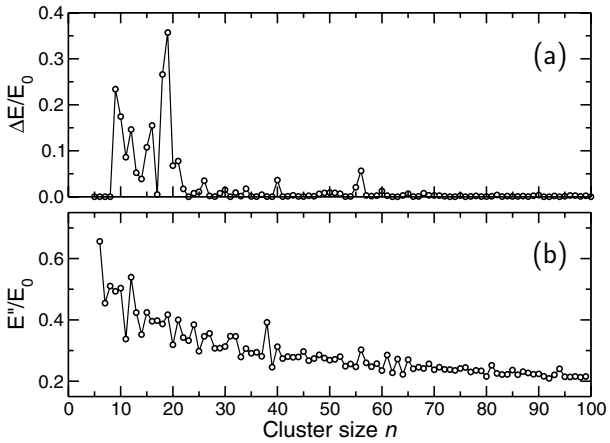

Fig. 1. (a) Energy gap $\Delta E(n) = E_2(n) - E_1(n)$ between the two lowest isomers and (b) second energy derivative $E''(n) = E(n+1)+E(n-1)-2E(n)$, for clusters in an isotropic harmonic trap, as a function of n.

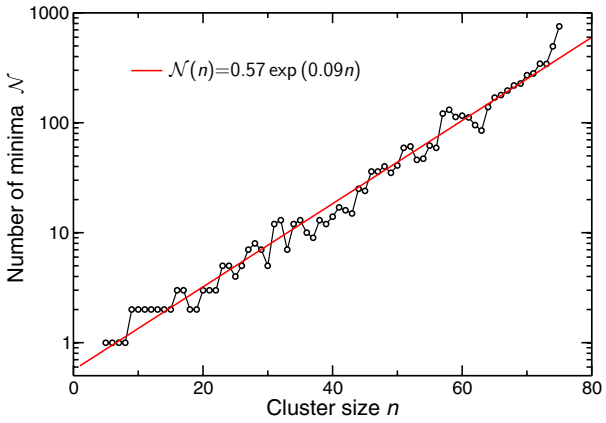

Fig. 2. Lower bound for the estimated number of minima for clusters in an isotropic trap, as a function of size. The straight line is an exponential fit.

stability of these global minima. Stability can be considered from different points of view. In a first approximation, the intrinsic thermodynamical stability is reflected by the energy gap $\Delta E(n) = E_2(n) - E_1(n)$ between the two lowest energy structures. As is customary in cluster physics, the stability of a particular size can also be quantified by comparing its binding energy to those of its neighbours, thus calculating the second energy derivative $E''(n) = E(n+1) + E(n-1) - 2E(n)$. The variations of these two indicators with the number of particles are represented in Figure 1.

The intrinsic thermodynamical stability characterized by ΔE mostly shows low values, in agreement with the work by Beekman et al. [22]. At small sizes, where there are only very few isomers, the energy gap may be significant. It is maximum at $n = 19$, which only has two isomers (1, 18) and (19), but very small at size 17, for which two different (1, 16) isomers exist in a narrow energy range. Above $n = 20$ only few sizes (notably 40 and 56) are particularly stable, even though for 60, whose ground state is (12, 48), we find a lower energy gap than in reference [22], resulting from a low (1, 12, 47) isomer. This suggests that our database of minima contains structures that are lower in energy than in the work by Beekman and coworkers [22].

The second energy difference $E''(n)$ in Figure 1b shows a general decreasing trend, not revealing any special stabilities. Marginal peaks are seen at $n = 12$, 38 and, to a lesser extent, 56. They are generally not correlated with the appearance of new shells: for instance, all global minima in the range 36–41 are based on the (6, p) motif. Neither do they match the variations in the energy gap $\Delta E(n)$ between the two lowest isomers, except maybe for size 56. Therefore the second energy difference is not expected to be very helpful in interpreting dynamical or thermodynamical data.

By repeating the basin-hopping search a large number of times for each cluster size, the database of isomers was seen to become stationary, hence we attempted to enumerate them, using the potential energy and mean square radius as identification criteria. The number $\mathcal{N}$ of minima is expected to grow exponentially with n, but this number is also primarily affected by the range of the interparticle potential [41,48], potentials with a shorter range leading to more numerous isomers. In the present case, the very long range of the Coulomb interaction tends to minimize the number of isomers, allowing us to estimate it by performing many thousands optimizations from random structures. The number of permutationally independent structures obtained this way is represented in Figure 2 as a function of cluster size.

Obviously, our basin-hopping search only provides a lower bound for the actual number of isomers. This is especially true for sizes above 70, for which a few more isomers were discovered during the last series of 10^4 quenches. This explains why we limited our search to size 75, without pretending our collections to be exhaustive in the range 60–75. However, for sizes up to 60, we believe not to have missed a large number of important structures.

Figure 2 clearly indicates that the number of permutationally independent isomers grows exponentially with cluster size, in agreement with the commonly accepted conjecture [47]. The coefficients for the exponential fit are rather small, and confirm that long-range potentials lead to fewer minima. For instance, 13 ions confined in a 3D harmonic trap exist in only two possible configurations, namely (1, 12) and (13). For comparison, the 13-atom Lennard-Jones cluster has more than 1500 different minima [41]. Thus, even though global optimization of the potential surface of equation (1) is a NP-hard problem, it is still much simpler than for other clusters with short range interactions, including Lennard-Jones or, worse, Girifalco or high ρ Morse potentials.

3.2 Isomerization and melting: selected cases

The finite-temperature simulations were performed in two ways. As is commonly used in the trapped ions community [25–28], standard constant-energy molecular dynamics trajectories were carried out to probe the dynamics

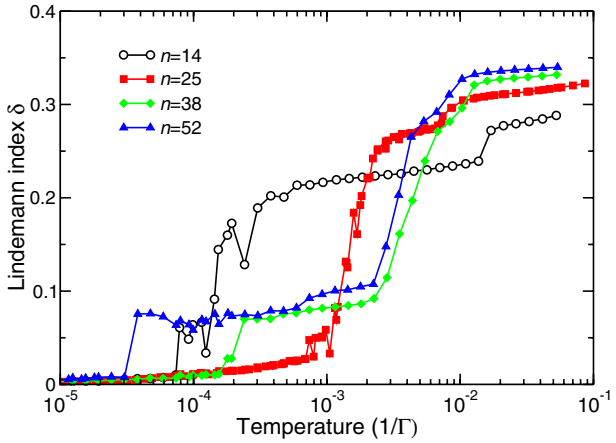

Fig. 3. (Color online) Variations of the Lindemann index δ as a function of temperature, obtained from molecular dynamics simulations for selected clusters in an isotropic trap.

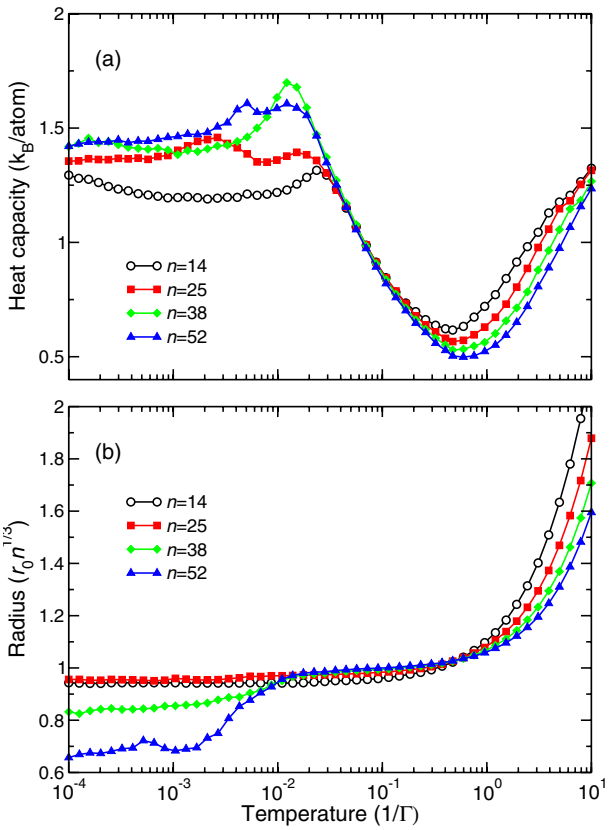

Fig. 4. (Color online) (a) Canonical heat capacities and (b) mean square radius of selected clusters in an isotropic trap, obtained from exchange Monte Carlo simulations. Note that the temperature range differs from that of Figure 3.

of melting. Here we calculate the root mean square bond length fluctuation index δ to quantify the level of rigidity in the cluster.

Monte Carlo simulations, improved with the all-exchange strategy [60], were also performed in the canonical ensemble to get insight into the purely thermodynamical behaviour of the clusters. This method was mainly used to compute the canonical heat capacity. In principle, both the MC and MD methods should give identical results, as far as they ergodically explore the configuration space. However, we use here the two methods to get complementary information. As was shown previously for the 2D problem [38], they do not necessarily agree with each other, which also reflects the different nature of the microcanonical and canonical ensembles for finite size systems.

All cluster sizes in the range $4 \leq n \leq 100$ have been investigated, and we first focus on some specific sizes, which were selected to illustrate various behaviours. Figure 3 shows the variations of the rms bond length fluctuation index δ with internal temperature of the clusters. Here the temperature is the microcanonical value obtained from the average of the kinetic energy in constant-energy molecular dynamics simulations, and it varies roughly linearly with total energy.

For the four selected clusters, δ shows similar variations, that is essentially four plateaus separated by three sharp rises. At very low temperatures, the clusters are in a rigidlike state and oscillate around their lowest energy structure. A first increase in the Lindemann index occurs to values generally close to $\delta = 0.07$, but lower in the case of $n = 25$ ($\delta \sim 0.04$). At this point the clusters become only partially rigid, and inspecting their structure reveals that the inner shells move with respect to each other. Above some higher temperature another steep rise in the Lindemann index expresses radial melting of the cluster. δ reaches then values close to 0.25. However, at even higher temperatures, another increase in δ occurs, with a somewhat broader character, leading to values in the range 0.27–0.34. This transition to an even more fluid state suggests that the previous state was still in a partially ordered state. In this respect, the multi-step melting process found here is comparable to what is seen in ionic clusters [44], in which actual melting is rather hard to detect on the variations of the Lindemann index alone.

The stability ranges of the intermediate phases of orientational and radial melting are strongly dependent on the number of particles. For instance, the smaller cluster $n = 14$ orientationally melts near $T \simeq 0.8 \times 10^{-4}$, and radially melts at $T \simeq 1.5 \times 10^{-4}$, while for the larger cluster $n = 52$ the orientationally melted phase sets at $T \simeq 0.4 \times 10^{-4}$ and ends at $T \simeq 3 \times 10^{-3}$. The melting temperatures, as defined from the increase of δ above 0.15, are thus strongly size-dependent, as expected from small finite systems [34], and in agreement with previous results on two-dimensional trapped ions [37,38]. By comparison, the temperature corresponding to the last increase in δ are much more stable against variations in size, and is always close to 10^{-2}.

The configurational canonical heat capacities $C_v(T)$ of the four selected clusters are shown in Figure 4a in the temperature range where they exhibit noticeable variations. To further interpret these data, we have also represented the variations of the thermally average cluster mean square radius, normalized by $N^{1/3}$ to enable comparison between the different sizes. As for the 2D case [38], the general shape of these curves illustrates the changes

from solid-like to liquid-like, then to gas-like phases hindered by the confinement. The large drop in C_v at temperatures near $T = 1$ is intrinsic to the potential $r^2 + 1/r$, and is found also for two-dimensional clusters.

At low temperatures, the heat capacity per particle reaches the classical Dulong-Petit limit $C_v/k_B \to (3n - 6)/2n = 3/2 - 3/n$. At higher temperatures $T > 10^{-2}$, a strong drop in the heat capacity marks the onset of the expansion of the cluster toward the gas phase, clearly visible on the variations of the cluster radius in Figure 4b. As the cluster expands, its becomes a gaslike fluid, in contrast with the infinite one-component plasma at fixed density which exhibits only a single phase transition. At very high temperatures, the ions behave independently of each other and the main interaction is that of the confinement. The radial distribution function is very flat in this regime, in agreement with Schiffer [27], hence the system can be effectively considered as a gas. For this gas of non interacting particles, equipartition holds again: $C_v/k_B \to (3n - 6)/2n$, as seen in Figure 4.

Between the solid-like and gas-like phases, one or several intermediate liquid-like phases occur, as indicated by corresponding features (peaks or bumps) in the heat capacity. With respect to the bulk [31] or even to large clusters [27], the heat capacity peak is strongly smeared out by the important size effects present in small clusters. They are also qualitatively different, showing bumps or even additional peaks. Such premelting features are not unusual in atomic clusters [42–46], where they are usually followed by the main melting peak. Here the preliminar bumps are rather spectacular in the cases of $n = 25$ and $n = 52$, where they are more intense than the final peak occurring near $T = 10^{-2}$. To our knowledge, only a very few examples of such exacerbated premelting phenomena have been reported in the literature [46,62]. This is another manifestation of the strong cluster size effects on thermodynamics.

Comparing now Figures 3 and 4 we find no signature of orientational melting on the heat capacity. This is actually not surprising, since orientational melting usually is expected to involve similar isomers based on the same radial structure. As will be shown below, this does not necessarily imply that the global minimum structure is the only isomer to be visited. But the very similar energies of the isomers involved in orientational melting do not lead to significant latent heats or bumps in the heat capacity, while they have strong consequences on the Lindemann index. The dynamical melting temperature, at which δ increases above 0.15, generally differs from the thermodynamical melting temperature where the heat capacity is maximum. However, we find that the temperature where the rms bond length fluctuation exhibits its last increase above 0.27–0.34 closely matches the temperature of the last peak in the heat capacity. At this temperature close to 10^{-2}, the reduced mean square radii of all clusters converge to about 0.95. This suggests a more robust definition of the melting temperature, which reconciles both dynamical and thermodynamical definitions, and naturally agrees in the bulk limit of the free one-component plasma.

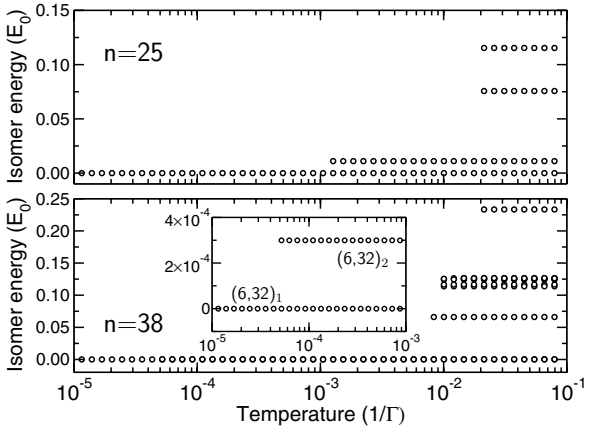

Fig. 5. Temperature-dependent isomer spectra obtained from quenching Monte Carlo trajectories, for clusters with $n = 25$ (upper panel) or $n = 38$ (lower panel) in an isotropic trap, as a function of temperature. For $n = 38$, the inset highlights the structural transition between the two first isomers, having both the (6, 32) radial composition.

To further analyse the caloric curves of Figure 4 in terms of the properties of the potential energy surface, especially its minima, we have performed systematic quenches of the MC trajectories, minimizing 1000 configurations for each replica. The isomers spectra are shown in Figure 5 for cluster sizes $n = 25$ and 38.

The 25-particle cluster has four distinct isomers, energetically ordered as (2, 23), (3, 22), (1, 24), and (4, 21), respectively. The heat capacity of this cluster shows two peaks at the temperatures 4×10^{-3} and 10^{-2}, respectively. These temperatures correspond only approximately to the onset of appearances of isomers 2 (near $T \sim 10^{-3}$) and 3 and 4 ($T \sim 2 \times 10^{-2}$). The quantitative disagreement between the peak temperatures and the appearance temperatures indicates that the entropy contributions of the isomers are important.

The case of the 38-particle cluster is quite interesting. For this system the global minimum is nearly degenerate with another isomer of the same radial composition, namely (6, 32). The corresponding transition between these isomers occurs around $T = 5 \times 10^{-5}$, and does not involve any significant latent heat, no peak being visible in the heat capacity. Most other isomers appear near $T = 10^{-2}$, consistently with the marked peak in C_v in Figure 4. The absence of signature of the preliminary structural transition on the variations of the Lindemann index is the consequence of the high energy barrier for rearrangement between the two isomers. Even though this rearrangement can be seen as a relative orientational motion between the two shells, the isomers involved are not accessed too early in the molecular dynamics simulations. This is therefore a case where the orientational motion can be hindered by significant barriers, such a situation which was first reported by Wales and Lee [21]. The MD simulations performed for this cluster at low energies cannot be ergodic when starting from the global minimum, until the total energy exceeds the energy barrier for rearrangement

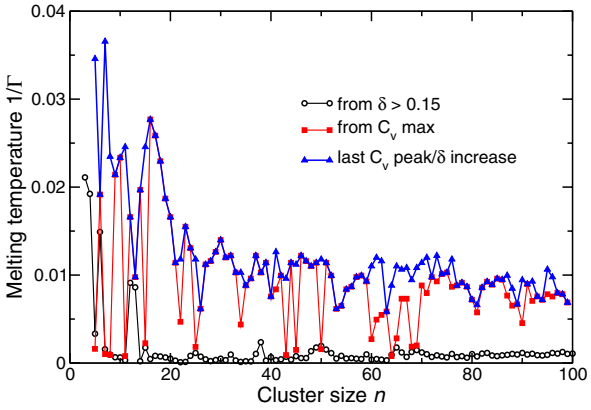

Fig. 6. (Color online) Melting temperatures of clusters in an isotropic trap, obtained from the basic Lindemann criterion $\delta > 0.15$ (empty squares), the absolute maximum in the heat capacity (full circles), or from its last maximum (triangles), as a function of size.

between the two lowest isomers. In contrast, the exchange Monte Carlo simulations are able to sample the equilibrium between accessible basins on the energy landscape without explicitly visiting the barrier regions.

3.3 Finite-size effects on the melting point

From the previous analysis, it seems clear that the two simulation methods used in this work do not exactly convey the same information, partly because they do not sample configuration space similarly. More importantly, they emphasize that a complete picture of the dynamics and thermodynamics of clusters of trapped ions cannot be obtained using one of these methods alone. This is obvious on the melting temperature, whose value critically depends on the way it is defined. In the four cases studied above, the standard Lindemann criterion and the usual thermodynamical definition based on the heat capacity maximum disagree significantly with each other. Agreement could only be reached by considering the highest-temperature increase of δ above 0.27 and maximum in C_v. This is in fact not specific to these four cases, but seems to hold for other cluster sizes as well. We have represented in Figure 6 the variations of the melting temperatures inferred from the standard Lindemann index ($\delta > 0.15$), the absolute maximum in the heat capacity, and the temperature of the highest-temperature peak in C_v, for all cluster sizes in the range $n \leq 100$.

The melting temperature based on the heat capacity absolute maximum systematically exceeds the dynamical melting temperature based on $\delta > 0.15$, by a typical order of magnitude. Only occasionally the two temperatures agree, within a factor 2–3, as in the cases of $n = 11$, 13, 15, 25, 43, 45, 50, 64, and 69. The two temperatures extracted from the heat capacity maxima often coincide, but not always. As seen on our previous four examples, the melting temperature should be more reliably defined from the last maximum in C_v, not from its absolute maximum. The variations of this quantity show a decreasing tendency, while the dynamical temperature based on δ shows an overall increase. As the cluster grows, it becomes more compact and the core shells resist better to orientational melting. Following previous work on atomic clusters [61, 63], melting at the finite-size scale is then expected to evolve toward a single-step, first-order like process where the highest-temperature peak is the highest, and the premelting and multi-step melting phenomena are attenuated.

The dynamical melting temperature of large sizes is about 2×10^{-3}, in agreement with the value of the critical parameter $\Gamma \sim 500$ reported by Schiffer for the 100-ion cluster [27], also obtained using MD simulations. The canonical heat capacity of this cluster shows a broad peak at this temperature, also with a similar height (latent heat), hence consistent with reference [27] as well. However, it exhibits another peak, higher and centered at $T \sim 7 \times 10^{-2}$, which again explains the different values found for $n = 100$ in Figure 6. Thus we believe that the simulations performed by Schiffer, though they partially agree with ours in a limited low-temperature range, are incomplete to reveal the actual melting point of this cluster.

Using any of the three definitions, the variations of the melting temperature with the number of particles is strongly non-monotonic. Interestingly, we do not find any particular correlation between the melting temperature extracted from the heat capacity and the energy gap ΔE shown in Figure 1a, suggesting that the peaks in C_v are caused by the sudden appearance of bunches of isomers. The relatively weak role of the specific second isomer was already illustrated above for $n = 52$. The melting temperature do not correlate much with the second energy difference, confirming the poor role of geometric magic numbers on these 3D trapped ions clusters.

3.4 Vibrational spectra

Several authors have experimentally or theoretically investigated the normal modes and vibrational frequencies of two-dimensional [49–53] and three-dimensional [54–57]. Recently, Nelissen and coworkers calculated the frequency spectrum of such planar clusters numerically, and interpreted their results with the solution of an hydrodynamical model due to Ye and Zaremba [64]. They found that some frequencies do not vary significantly with the number of particles, and that these frequencies are generally associated with low vorticity eigenvectors.

The hydrodynamic theory for three-dimensional clusters [54] treats the system as a cold fluid, and predicts that incompressible modes of spheroidal shapes are characterized by the set of frequencies ω_ℓ, for integers $\ell > 0$:

$$\omega_\ell^2 = \frac{\ell}{2\ell + 1}\omega_p^2, \tag{4}$$

where $\omega_p = 3\omega_0$ is the frequency for compressible modes, also known as the plasma frequency. The normal modes

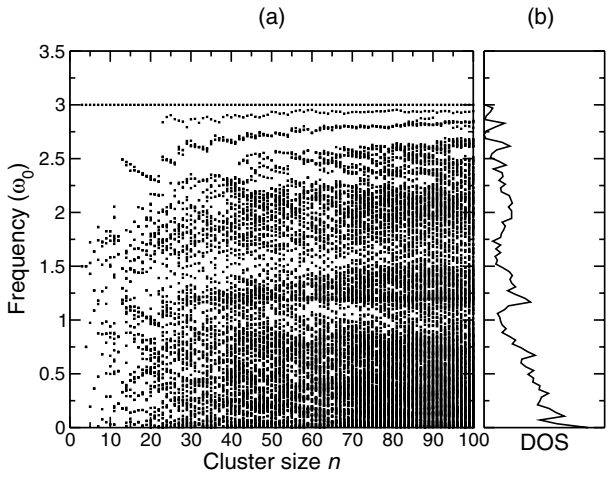

Fig. 7. (a) Vibrational spectrum of the lowest-energy structure for clusters in an isotropic trap, as a function of size. (b) Density of vibrational states accumulated for sizes $90 \leq n \leq 100$.

are fully described by Dubin and Schiffer [54,55] within cold fluid theory. Each mode ℓ is further characterized by another quantum number m varying between $-\ell$ and $+\ell$, which determines the degree of variation of the mode potential. According to hydrodynamic theory, all vibrational frequencies thus lie in the range $\sqrt{3}\omega_0 \leq \omega \leq 3\omega_0/\sqrt{2}$.

We have calculated the spectrum of vibrational frequencies $\{\omega_i\}$ of the present 3D clusters by diagonalizing the second derivative matrix of potential energy. The spectra are represented in Figure 7a as a function of n. As for the 2D case, some frequencies seem to be always present for all sizes. Besides the six zero eigenvalues corresponding to global translations and rotations, the breathing mode $\omega = 3\omega_0 = \omega_p$ is seen as an horizontal line. Conversely to the two-dimensional case, the frequency spectrum is bounded from above by the breathing mode $\omega = 3$, in agreement with cold fluid continuous theory [54].

On the right (b) panel of Figure 7, the density of vibrational states obtained by accumulating the spectra for sizes in the range $90 \leq n \leq 100$ reveals that more and more modes grow near $\omega = 1.2\omega_0$ and $\omega = 2\omega_0$, and even more at low frequencies $\omega \to 0$. This is another important contrast with the two-dimensional situation, in which the relative density of low frequency modes was seen to decrease at large n [52]. There are no accumulation of modes toward $\omega_p/\sqrt{2}$, as is predicted by the hydrodynamic theory for large sizes and $\ell \to \infty$. This indicates that, at the scale of the present clusters $n \leq 100$, cold fluid theory may not yet be appropriate for describing elementary vibrations. We can also compare the present DOS with the densities numerically calculated by Dubin and Schiffer for a 1000-particle cluster, and for the periodic fcc and bcc one-component plasma [55]. These authors found essentially similar shapes for the DOS, with two main broad peaks centered around $0.9\omega_0$ and $2.8\omega_0$. For the finite system, the additional surface modes appear near $3\omega_0/\sqrt{2}$, in agreement with cold fluid theory [54]. The density accumulated here for clusters having between 90 and 100 particles shows a very different shape, with an exceedingly large number of low-frequency modes, and no clear signature of the surface modes.

Table 1. Breathing frequency and associated rank for icosahedral atomic Lennard-Jones clusters. The frequency is given in reduced LJ units.

Cluster	Breathing frequency	Rank
LJ_{13}	15.1	4/33
LJ_{55}	10.9	101/159
LJ_{147}	8.4	376/435
LJ_{309}	6.9	871/921
LJ_{561}	5.8	1627/1677

That the breathing mode is the hardest is not a general feature of trapped ion clusters: this feature is not present in two-dimensional clusters. Neither is it a property of general three-dimensional clusters. We have calculated the vibrational spectra of atomic clusters bound by Lennard-Jones forces, and identified the rank n of the breathing mode among the entire spectra of k modes. Here the rank n/k is defined for increasingly hard modes, hence rank $1/k$ means that the breathing mode is the hardest, and k/k means the softest. The breathing frequency (in Lennard-Jones units) and the associated rank are given in Table 1 for a selection of icosahedral LJ clusters.

The above results for LJ clusters were confirmed by looking at other clusters bound by ionic (sodium fluoride) or many-body (sodium) forces, and by adding an harmonic trap. By minimizing random structures of 3D trapped ion clusters containing up to 1000 particles, we have checked that all frequencies are indeed lower than 3. This property does not hold when the interaction between particles has a shorter or a longer range than the bare Coulomb interaction, therefore it results from the specific combination of dimensionality and interaction potential, as well as the presence of the harmonic trap. This property is consistent with the predictions of hydrodynamic theory [54].

4 Clusters confined in anisotropic traps

In experiments built with the linear Paul trap, the radiofrequency can be tuned to change the shape of the ion clouds [7,8]. Such shape transitions were already discussed in the light of early molecular dynamics simulations [18, 25,58]. In particular, Schiffer [58] investigated systematically the critical anisotropy parameters at which the stable structure evolves from linear to zigzag, then helicoidal, three-dimensional, and eventually planar. His results were soon after analytically interpreted by Dubin who approximated the clusters with a homogeneous continuous distribution [17].

4.1 Finite size effects on the shape diagram

In their respective works, Schiffer [58] and Dubin [17] investigated the general properties of shapes and shape transitions in a broad range of cluster sizes. Here we have repeated the optimizations of Schiffer, by looking at all

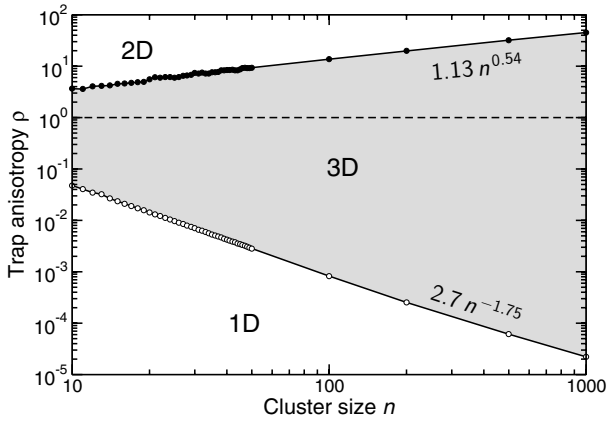

Fig. 8. Shape diagram for clusters in an anisotropic trap. For increasing anisotropy ρ, the clusters change from quasi linear (1D), to ellipsoids (3D), to planar (2D). The two straight lines are fits from the numerically determined critical anisotropies at particular sizes in the range $n \leq 1000$.

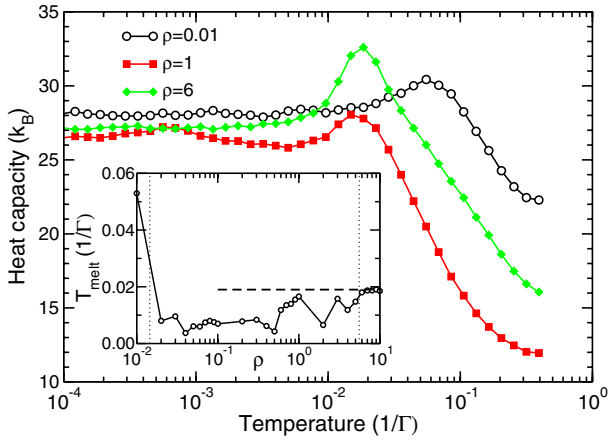

Fig. 9. (Color online) Heat capacities for the 20-particle cluster in an anisotropic trap, for several anisotropy ratios ρ. The variations of the melting point with ρ are given in the inset, the horizontal dashed line being the result for perfectly planar clusters ($\rho \to \infty$). In the inset also, the vertical dotted lines indicate the critical values for the 1D $\to$ 3D and 3D $\to$ 2D shape transitions.

sizes n up to 50, and several larger sizes, aiming at evidencing possible finite-size effects. For each size, the global minimum obtained for the isotropic trap was further minimized for increasing or decreasing ρ. Planar configurations were detected using the definition $\max(|z_i|) < 0.1$. Similarly, linear configurations are defined according to $\max(\sqrt{x_i^2 + y_i^2}) < 0.1$. We do not distinguish here between the purely linear, zigzag, and helicoidal configurations, which are not expected to give rise to strong finite size effects.

The global shape diagram we calculated is represented in Figure 8. The 1D $\to$ 3D $\to$ 2D shape transitions are correctly characterized by approximate scaling laws, whose exponents agree well with those of references [17,58]. The logarithmic corrections suggested by Dubin for the 1D $\to$ 3D transition are probably not important yet at the size $n = 1000$. In the range $n \leq 50$, the particle-resolved finite size effects are rather weak in general, especially for the 1D $\to$ 3D transition at low anisotropies. The planar transition is slightly more affected, some deviations around the power law $\rho_{2D}(n) = 1.13n^{0.54}$ being seen near $n = 21$.

The present results show that the shape of the clusters is not too sensitive with respect to the exact number of particles, and that it essentially follows the laws of an incompressible fluid [17].

4.2 Influence of anisotropy on the caloric curves

While the trap anisotropy smoothly influences the shape of a cluster of trapped ions, it has stronger consequences on its thermal stability. We have determined the global minimum of the specific cluster size $n = 20$ for increasing values of ρ across the 1D $\to$ 3D and 3D $\to$ 2D transitions. The isotropic 20-particle cluster has a relatively high thermodynamical melting temperature $T_{\rm melt} \simeq 0.016$. We have carried out exchange Monte Carlo simulations for an anisotropy parameter spanning 30 values in the range $10^{-2} \leq \rho \leq 10$, the two shape transitions occurring near $\rho_{1D} \simeq 0.015$ and $\rho_{2D} \simeq 5.45$, respectively. We did not attempt to use molecular dynamics simulations for anisotropic traps, due to the non conservation of angular momentum resulting from the loss of rotational invariance.

Three typical heat capacity curves are shown in Figure 9 for $\rho = 10^{-2}$, 1, and 6, corresponding to 1D, 3D, and 2D shapes, respectively. The anisotropy of the trap has dramatic consequences on the caloric curves. For a large part, these effects are due to changes in the stable structures and the ordering between isomers. In particular, the number of isomers itself is strongly affected by ρ. This is particularly obvious at low anisotropies: the 1D cluster has a single isomer and exhibits a single solid-gas transition without a real intermediate liquid phase. This explains its rather high melting temperature, close to 0.054. As the anisotropy of the trap crosses 1.5×10^{-2}, the cluster becomes three-dimensional, but remains as a prolate ellipsoid until ρ equals 1. In the isotropic case, premelting effects are visible on the heat capacity, which exhibits a broad bump centered around $T \simeq 6.3 \times 10^{-4}$. At $\rho = 6$, the cluster is planar, and shows a single step melting process with a rather high and narrow peak near $T = 0.019$.

The size effects on the dependence of cluster properties with respect to ρ are magnified in the inset of Figure 9, where the variations of the melting point, defined from the highest temperature C_v peak in case several are present, are represented as a function of ρ. In the 3D regime, that is for $0.015 \leq \rho \leq 5.45$, the change in the number of isomers and their relative energies and entropies yields significant changes in the melting temperature, especially near $\rho \sim 0.5$ and $\rho \sim 1{-}2$. However, as the cluster becomes oblate, its melting point smoothly converges to that of the bidimensional system found at $\rho \to \infty$ [38]. This is not true for the 1D case obtained at low ρ, because

the distance between neighbouring particles diverges as $\rho \to 0$ [17].

The variations in the melting point with the trap anisotropy are non trivial, and we expect them to be also dependent on the number of particles, as was previously shown in the case of the isotropic trap. This will prevent one from constructing a detailed and quantitative (n, ρ) diagram at various temperatures, but it would be interesting to study the effects of ρ on the melting of larger clusters.

5 Conclusions

Clusters of identical charged particles confined by harmonic traps exhibit structural, dynamical, and thermodynamical properties that strongly depend on the trap anisotropy, the temperature, and the number of particles itself. In the present work, we have addressed these issues using numerical MC and MD simulations, for clusters containing up to 100 ions. The relative stabilities of the global minima, estimated by computing the second energy difference, did not reveal any significant extra stabilities that could reveal the completion of geometrical shells. The thermal stability of the global minimum, as roughly quantified by the energy gap between the two lowest energy isomers, tends to be rather weak as well, especially for sizes above 20.

The long range forces that operate for the present clusters yield a rather small number $\mathcal{N}$ of permutationally independent isomers at a given size, compared to e.g. Lennard-Jones clusters. A lower bound for this number was found as $\mathcal{N}(n) \geq 0.57e^{0.09n}$, in agreement with the expected exponential increase of inherent structures [41,47]. While a more exhaustive sampling of minima could probably be achieved using global optimization tricks such as taboo search, we stress that our enumeration stands as the first for clusters of trapped ions. The effects of dimensionality, trap anisotropy, and the range of the potential could be investigated in the future.

Our results on the finite-temperature dynamics and thermodynamics emphasized the very strong finite size effects exhibited by such small clusters. As in the case of two-dimensional species [38], both the Lindemann index and the heat capacity show several steps or bumps, respectively, at increasing temperatures. We found the standard definitions of the cluster melting point, based either on the Lindemann index exceeding 0.15 or the heat capacity being absolutely maximum, to be inconsistent with each other. This reflects the different mechanisms probed by the two parameters. The Lindemann index is sensitive to orientational melting, which generally (but not always) takes place at very low temperatures due to the low energy barriers [21], then to radial melting, possibly in a multistep way. The canonical heat capacity, computed using the more ergodic exchange Monte Carlo method, is sensitive to the different minima and their ordering, and can exhibit premelting peaks more intense than the actual melting peak found at a higher temperature. Comparing the variations of δ, C_v and the thermally averaged mean square radius, we propose to define the cluster melting point as the temperature corresponding to the last (or highest temperature) increase in the Lindemann index above 0.27, or the last peak in the heat capacity. This definition seems to generally reconcile the two indicators, a result which was overlooked in our previous work on 2D clusters [38].

In some cases ($n = 38$), different isomers are accessible at very low temperatures without being seen on the variations of the Lindemann index. Therefore the cluster behaviour cannot be fully interpreted from a single of the two methods and indicators. This seems an important word of caution to the use of molecular simulation of finite size systems, as neither the MD or the MC method are guaranteed to give the same information, but instead they provide complementary data.

The variations of the melting point with increasing number of particles have been obtained for clusters containing up to $n = 100$ particles. These variations are non-monotonic, but their fluctuations tend to decrease for large clusters, as expected. The quantitative difference with the melting point reported for the 100-particle cluster by Schiffer [27] may be due to our finding of an extra heat capacity peak at a higher temperature. Our value for the melting point does not match the scaling law inferred by this author from its numerical results on larger clusters. This could be due to the structural transition known to take place around 10^4 ions between shell-structured global minima and surface-relaxed bcc lattices geometries [23].

The vibrational spectrum was calculated as a function of cluster size, up to the size 100. As in the 2D case, some frequencies remain constant (the plasma frequency $\omega = 3\omega_0$ for breathing) or accumulate near fixed values ($\omega = 1.2\omega_0$ or $2\omega_0$). However, the accumulation of modes toward low frequencies is in clear contrast with the 2D case [52], and we do not find evidence in the small clusters studied here for incompressible surface modes with frequencies in the range $\sqrt{3}\omega_0 \leq \omega \leq 3\omega_0/\sqrt{2}$, that are predicted by the hydrodynamical theory [54]. This indicates that the correlations between particles, which are not taken into account in the cold fluid theory [54], are strongly important in the low-size regime [55,56].

Finally, we have investigated the case of anisotropic traps, first looking at the finite size effects on the shape of the lowest energy structure. While the general shape diagram agrees with early investigations by Schiffer [58] and Dubin [17], we found no evidence for strong size effects on the values of ρ at which the cluster becomes essentially one-dimensional or planar. In contrast, the effects of changing the anisotropy were seen to be much more significant on the heat capacity curves, resulting in strong anisotropy-dependent melting points. The thermodynamics of larger, nonspherical clusters could well depend on the anisotropy parameter ρ as well, but probably more smoothly. Recently, Komatsu and Abe found that evaporation was easier in nonspherical clusters, the emission of particles being favored at the tips [65]. This could also be the case for the present trapped ion clusters, but such an investigation would require large numbers of particles ($n \sim 1000$) in order to minimize the very strong cluster size effects found here in the small size regime.

F.C. would like to thank Dr. C. Champenois for fruitful discussions. We are also grateful for a collaborative research grant given by CNRS and TUBITAK.

References

1. W.M. Itano, J.J. Bollinger, J.N. Tan, B. Jelenkovic, X.-P. Huang, D.J. Wineland, Science **279**, 686 (1998); T.B. Mitchell, J.J. Bollinger, D.H.E. Dubin, X.-P. Huang, W.M. Itano, R.H. Baughman, Science **282**, 290 (1998)
2. M. Drewsen, C. Brodersen, L. Hornekær, J.S. Hangst, J.P. Schiffer, Phys. Rev. Lett. **81**, 2878 (1998)
3. O. Arp, D. Block, A. Piel, A. Melzer, Phys. Rev. Lett. **93**, 165004 (2004)
4. M. Drewsen, A. Brøner, Phys. Rev. A **62**, 045401 (2000)
5. A. Mortensen, E. Nielsen, T. Matthey, M. Drewsen, Phys. Rev. Lett. **96**, 103001 (2006)
6. L. Hornekær, N. Kjærgaard, A.M. Thommesen, M. Drewsen, Phys. Rev. Lett. **86**, 1994 (2001)
7. N. Kjærgaard, K. Mølhave, M. Drewsen, Phys. Rev. E **66**, 015401 (2002); N. Kjærgaard, M. Drewsen, Phys. Rev. Lett. **91**, 095002 (2003)
8. M. Drewsen, I.S. Jensen, N. Kjærgaard, J. Lindballe, A. Mortensen, K. Mølhave, D. Voigt, J. Phys. B: At. Mol. Opt. Phys. **36**, 525 (2003)
9. K. Mølhave, M. Drewsen, Phys. Rev. A **62**, 011401(R) (2000)
10. N. Hermanspahn, H. Häffner, H.-J. Kluge, W. Quint, S. Stahl, J. Verdú, G. Werth, Phys. Rev. Lett. **84**, 427 (2000)
11. S. Bize, S.A. Diddams, U. Tanaka, C.E. Tanner, W.H. Oskay, R.E. Drullinger, T.E. Parker, T.P. Heavner, S.R. Jefferts, L. Hollberg, W.M. Itano, J.C. Berqquist, Phys. Rev. Lett. **90**, 150802 (2003)
12. D. Kielpinski, B.E. King, C.J. Myatt, C.A. Sackett, Q.A. Turchette, W.M. Itano, C. Monroe, D.J. Wineland, W.H. Zurek, Phys. Rev. A **61**, 032310 (2000)
13. J.A. Cirac, P. Zoller, Phys. Rev. Lett. **74**, 4091 (1995)
14. J. Bollinger, D. Wineland, Phys. Rev. Lett. **53**, 348 (1984); S.L. Gilbert, J.J. Bollinger, D.J. Wineland, Phys. Rev. Lett. **60**, 2022 (1988)
15. M. Bonitz, D. Block, O. Arp, V. Golubnychiy, H. Baumgartner, P. Ludwig, A. Piel, A. Filinov, Phys. Rev. Lett. **96**, 075001 (2006)
16. E.V. Baklanov, V.P. Chebotayev, Appl. Phys. B **39**, 179 (1986)
17. D.H.E. Dubin, Phys. Rev. Lett. **71**, 2753 (1993)
18. R. Rafac, J.P. Schiffer, J.S. Handst, D.H.E. Dubin, D.J. Wales, Proc. Natl. Acad. Sci. USA **88**, 483 (1991)
19. R.W. Hasse, V.V. Avilov, Phys. Rev. A **44**, 4506 (1991)
20. E.L. Alschuler, T.J. Williams, E.R. Ratner, F. Dowla, F. Wooten, Phys. Rev. Lett. **72**, 2671 (1994); E.L. Alschuler et al., Phys. Rev. Lett. **74**, 1483 (1995)
21. D.J. Wales, A.M. Lee, Phys. Rev. A **47**, 380 (1993)
22. R.A. Beekman, M.R. Roussel, P.J. Wilson, Phys. Rev. A **59**, 503 (1999)
23. H. Totsuji, T. Kishimoto, C. Totsuji, K. Tsuruta, Phys. Rev. Lett. **88**, 125002 (2002)
24. H. Totsuji, C. Totsuji, T. Ogawa, K. Tsuruta, Phys. Rev. E **71**, 045401(R) (2005); H. Totsuji, T. Ogawa, C. Totsuji, K. Tsuruta, Phys. Rev. E **72**, 036406 (2005)
25. A. Rahman, J.P. Schiffer, Phys. Rev. Lett. **57**, 1133 (1986)
26. D.H.E. Dubin, T.M. O'Neil, Phys. Rev. Lett. **60**, 511 (1988)
27. J.P. Schiffer, Phys. Rev. Lett. **88**, 205003 (2002)
28. T. Matthey, J.P. Hansen, M. Drewsen, Phys. Rev. Lett. **91**, 165001 (2003)
29. E.L. Pollock, J.P. Hansen, Phys. Rev. A **8**, 3110 (1973)
30. S. Ichimaru, Rev. Mod. Phys. **54**, 1017 (1982)
31. R.T. Farouki, S. Hamaguchi, Phys. Rev. E **47**, 4330 (1993)
32. P. Pawlow, Z. Phys. Chem. **65**, 545 (1909)
33. See, e.g. C.E. Bottani, A. Li Bassi, B.K. Tanner, A. Stella, P. Tognini, P. Cheyssac, R. Kofman, Phys. Rev. B **59**, 15601(R) (1999) and references therein
34. J. Jortner, Z. Phys. D: At. Mol. Clusters **24**, 247 (1992)
35. M. Schmidt, R. Kusche, B. von Issendorff, H. Haberland, Nature **393**, 238 (1998)
36. V.M. Bedanov, F.M. Peeters, Phys. Rev. B **49**, 2667 (1995)
37. J.A. Drocco, C.J. Olson Reichhardt, C. Reichhardt, B. Jankó, Phys. Rev. E **68**, 060401(R) (2003)
38. E. Yurtsever, F. Calvo, D.J. Wales, Phys. Rev. E **72**, 026110 (2005)
39. T.L. Beck, R.S. Berry, J. Chem. Phys. **88**, 3910 (1988)
40. D.J. Wales, Science **271**, 925 (1996)
41. D.J. Wales, *Energy Landscapes* (Cambridge University, Cambridge, 2003)
42. H.-P. Cheng, R.S. Berry, Phys. Rev. A **45**, 7969 (1992); F. Calvo, P. Labastie, Chem. Phys. Lett. **248**, 233 (1996)
43. E.G. Noya, J.P.K. Doye, J. Chem. Phys. **124**, 104503 (2006)
44. F. Calvo, P. Labastie, J. Phys. Chem. B **102**, 2051 (1998)
45. J.P.K. Doye, D.J. Wales, Phys. Rev. Lett. **80**, 1357 (1998); J.P. Neirotti, F. Calvo, D.L. Freeman, J.D. Doll, J. Chem. Phys. **112**, 10340 (2000)
46. V.A. Mandelshtam, P.A. Frantsuzov, J. Chem. Phys. **124**, 204511 (2006)
47. F.H. Stillinger, Phys. Rev. E **59**, 48 (1999)
48. P.A. Braier, R.S. Berry, D.J. Wales, J. Chem. Phys. **93**, 8745 (1990)
49. A. Melzer, M. Klindworth, A. Piel, Phys. Rev. Lett. **87**, 115002 (2001)
50. S.G. Amiranashvili, N.G. Gusein-zade, V. Tsytovich, Phys. Rev. E **64**, 016407 (2001)
51. S.W.S. Apolinario, B. Partoens, F.M. Peeters, Phys. Rev. E **72**, 046122 (2005)
52. K. Nelissen, A. Matulis, B. Partoens, M. Kong, F.M. Peeters, Phys. Rev. E **73**, 016607 (2006)
53. T.E. Sheridan, J. Phys. D: Appl. Phys. **39**, 693 (2006)
54. D.H.E. Dubin, Phys. Rev. Lett. **66**, 2076 (1991)
55. D.H.E. Dubin, J.P. Schiffer, Phys. Rev. E **53**, 5249 (1996)
56. D.H.E. Dubin, Phys. Rev. E **53**, 5268 (1996)
57. G. Téllez, Phys. Rev. E **55**, 3400 (1997)
58. J.P. Schiffer, Phys. Rev. Lett. **70**, 818 (1993)
59. D.J. Wales, J.P.K. Doye, J. Phys. Chem. A **101**, 5111 (1997)
60. F. Calvo, J. Chem. Phys. **123**, 124106 (2005); P. Brenner, C.R. Sweet, D. VonHandorf, J.A. Izaguirre, J. Chem. Phys. **126**, 074103 (2007)
61. P. Labastie, R.L. Whetten, Phys. Rev. Lett. **65**, 1567 (1990)
62. F. Calvo, F. Spiegelman, J. Chem. Phys. **120**, 9684 (2004)
63. F. Calvo, F. Spiegelmann, Phys. Rev. Lett. **82**, 2270 (1999)
64. Z.L. Ye, E. Zaremba, Phys. Rev. B **50**, 17217 (1994)
65. N. Komatsu, T. Abe, Phys. Rev. E **72**, 021601 (2005)